

## Ion implantation of rare-earth dopants in ferromagnetic thin films

V. Dasgupta,<sup>a)</sup> N. Litombe, and W. E. Bailey<sup>b)</sup>

*Materials Science Program, Department of Applied Physics, Columbia University, 500 West 120th Street, New York, New York 10027*

H. Bakhru

*College of Nanoscale Science and Engineering, SUNY Albany, 251 Fuller Road, Albany, New York 12203*

(Presented on 1 November 2005; published online 27 April 2006)

We show that high-dose ion implantation can be used to introduce rare-earth dopants for the control of precessional dynamics in magnetic thin films. Tb and Gd ions have been implanted in Ni<sub>81</sub>Fe<sub>19</sub> through Ta masks at dosages from  $1 \times 10^{14}/\text{cm}^2$  to  $1 \times 10^{15}/\text{cm}^2$ . Effects on dynamics are found to be similar to those contributed by cosputtered Tb and Gd dopants in Ni<sub>81</sub>Fe<sub>19</sub> (50 nm). Broadband ferromagnetic resonance measurements from 0 to 18 GHz show that adjustments in damping  $\alpha$  from 0.008 to 0.040 are fully intrinsic (Gilbert type) and roughly proportional to dose. The technique enables the creation of films with spatially modulated precessional characteristics.  
© 2006 American Institute of Physics. [DOI: [10.1063/1.2173212](https://doi.org/10.1063/1.2173212)]

### INTRODUCTION

Magnetization dynamics control attainable data rates in data storage and spin electronics. Issues related to precessional dynamics become more relevant as data rates approach 1 GHz, the domain of precessional frequencies  $f_p$  and relaxation rates  $\lambda = \gamma\mu_0 M_s \alpha$ , where  $\alpha$  is the dimensionless damping constant. Control of materials parameters involved in precession, such as the damping  $\alpha$ , effective gyromagnetic ratio  $g_{\text{eff}}$ , and anisotropy  $H_k$ , can be used to create nanostructures which respond and converge more quickly to pulsed applied fields.<sup>1</sup>

In previous work, we have shown that small quantities of rare-earth (RE) dopants (< 10%), introduced by cosputtering, strongly affect both precessional frequency and damping of Ni<sub>81</sub>Fe<sub>19</sub> thin films.<sup>1</sup> The enhanced damping arises from enhanced coupling between the Ni<sub>81</sub>Fe<sub>19</sub> spin moment and the lattice, mediated by the RE orbital moment.<sup>2</sup> Spin-lattice damping is expected to be of Gilbert type,<sup>3</sup> where the field linewidth  $\Delta H_{pp}$  should increase proportionally with frequency. Moreover, the energy transfer involved in this damping is localized to the dopant atom, and can therefore be localized to the extent that the dopant atom locations can be controlled.

In the semiconductor industry, ion implantation is widely used to localize dopant concentrations < 0.1% with submicron precision.<sup>4</sup> In magnetic device technology, ion implantation is less widespread, and mostly known as a source of controlled damage or heating. Ga implantation has been used as a means to locally suppress ferromagnetism.<sup>5,6</sup> Damage has been inferred in small devices formed by focused ion beams.<sup>7</sup> The constructive role of He<sup>+</sup> ion irradiation to manipulate anisotropy, either exchange<sup>8</sup> or uniaxial,<sup>9</sup> through local magnetic field annealing, has been pointed out.

In this paper, we show that ion implantation can be useful for the introduction of “active” impurities in ferromag-

nets. The sensitivity of damping  $\alpha$  and anisotropy  $H_k$  to small concentrations of Tb and Eu dopants, respectively, enables doses attainable through ion implantation to produce beneficial effects. We find that the implanted RE ions produce changes in the damping  $\alpha$  which are consistent with findings from cosputtered films, and can be seen to be Gilbert type, consistent with intrinsic spin-lattice coupling. The implanted ions appear to retain their functional characteristics.

### EXPERIMENT

Ni<sub>81</sub>Fe<sub>19</sub> (25 nm) thin films were deposited on glass substrates (25 × 25 mm<sup>2</sup>) using ion beam sputtering at a base pressure of  $1.0 \times 10^{-7}$  Torr. Magnetic anisotropy was induced using a static magnetic field of 20 Oe applied along the center conductor, creating an effective uniaxial anisotropy field  $H_k$ . Films were capped with Ta (15 nm), the thickness of which was selected for optimal dopant uniformity, according to molecular dynamics SRIM calculations.

Ion implantation of Tb and Gd was carried out using the 1 MV tandem accelerator at SUNY Albany. Tb and Gd ions were produced from evaporation of elemental charges. The implant energy was 220 keV, with Tb doses of  $1 \times 10^{14}/\text{cm}^2$ ,  $5 \times 10^{14}/\text{cm}^2$ , and  $1 \times 10^{15}/\text{cm}^2$ . A Gd dose was compared at of  $1 \times 10^{14}/\text{cm}^2$ . Implant times ranged from 2–24 h. Implanted ions entered through the Ta layer. Samples were rotated and water cooled during ion implantation.

The implanted Ni<sub>81</sub>Fe<sub>19</sub> films were characterized using broadband ferromagnetic resonance (FMR) measurements from 2–16 GHz. Measurements were carried out for in-plane resonance at room temperature, biased along the anisotropy axis defined in deposition. rf fields were delivered to the sample as in PIMM measurements,<sup>10</sup> substituting a cw microwave source for the pulse generator. Sample surfaces were passivated by several micrometers photoresist and placed on top of a lithographic coplanar waveguide (CPW) with 100  $\mu\text{m}$  center conductor width. Microwave fields of

<sup>a)</sup>Electronic mail: [vd2110@columbia.edu](mailto:vd2110@columbia.edu)

<sup>b)</sup>URL: <http://magnet.ap.columbia.edu>

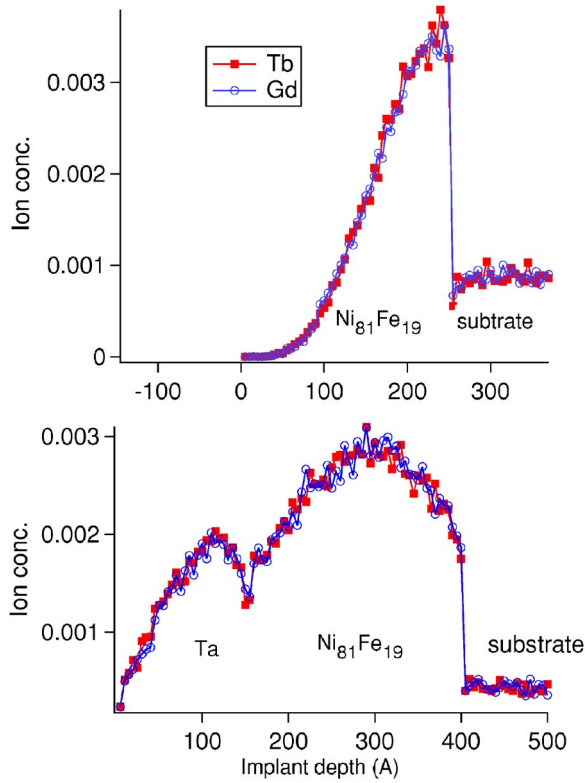


FIG. 1. (Color online) Simulation result (SRIM): concentration profile of Tb and Gd dopants implanted in  $\text{Ni}_{81}\text{Fe}_{19}$  at 220 keV. Top: no Ta layer. Bottom: 15 nm Ta layer. The Ta layer creates a more homogeneous distribution of RE dopants in  $\text{Ni}_{81}\text{Fe}_{19}$ .

0–18 GHz were applied using a synthesized sweep generator at 10–15 dBm. Transmitted intensity was measured at a microwave diode using lock-in techniques, synchronized with a 160 Hz ac magnetic field of 3 G rms applied using Helmholtz coils.

## RESULTS

The role of the Ta cap was explored using molecular dynamics (SRIM) simulation.<sup>11</sup> A characteristic of energetic ion interactions with atoms is the very sensitive dependence of stopping cross section upon ion energy. For 220 keV Tb or Gd ions implanted in Ni or Ta, ions undergo inelastic collisions as they pass through the material which increase the stopping probability as a function of depth. When no Ta layer is present, the implanted Tb stopping probability increases monotonically away from the top surface, leading to a monotonic increase in incorporated concentration. This can be seen in the top part of Fig. 1.

When a 15 nm Ta layer is incorporated, the ion concentration exhibits the same behavior in first part of the Ta layer, but the beam becomes depleted enough in Tb or Gd for the incorporated concentration to decrease thereafter. The same behavior is repeated in the  $\text{Ni}_{81}\text{Fe}_{19}$  layer with a lower energy threshold compared with the Ta layer. The calculated Tb/Gd concentration is roughly symmetric through the  $\text{Ni}_{81}\text{Fe}_{19}$  film, with a peak in the center, and is depleted at the top and bottom of the film by 30% of total dopant concentration.

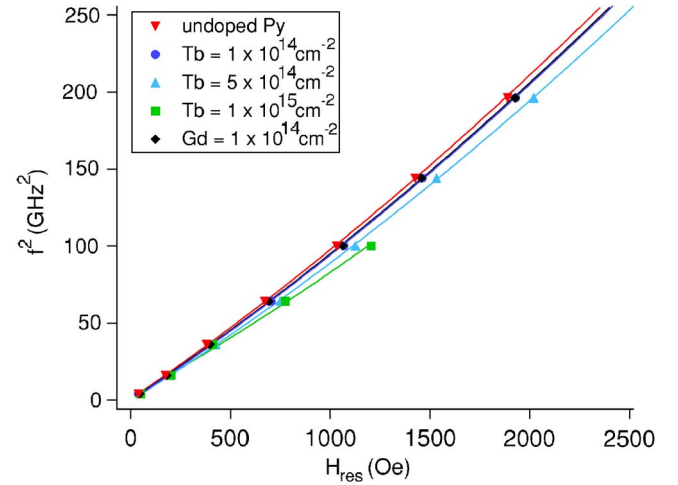


FIG. 2. (Color online) Kittel plot: solid lines are fits of Eq. (1) with saturation moment and anisotropy as free parameters (see Table I).

After implantation, the implanted films and one untreated  $\text{Ni}_{81}\text{Fe}_{19}$  (25 nm)/Ta (15 nm) control were characterized using FMR. We have used the relationship between applied field  $H$  and FMR frequency  $f$  to estimate magnetic moments  $B_s$ , and anisotropy  $H_k$  in the films, according to the Kittel equation,

$$\omega = \mu_0 \gamma_0 g_{\text{eff}} \sqrt{(M_s + H + H_k)(H + H_k)}, \quad (1)$$

where  $\gamma_0 g_{\text{eff}}$  is the gyromagnetic ratio, 175.86 GHz/T for  $g_{\text{eff}}=2$ . Plots of experimental data with fits to Eq. (1), using  $M_s$  and  $H_k$  as free parameters, are shown in Fig. 2, for all samples. Plots are given as  $f^2$  vs  $H$  to show the low-field  $H \ll M_s$  linearity  $f^2 \approx \gamma_0^2 / (2\pi)^2 g_{\text{eff}}^2 B_s (\mu_0 H + \mu_0 H_k)$ .

An obvious decrease in slope can be perceived for the higher dose Tb samples, while the offset in field does not change noticeably. According to the approximate relation, the change in slope implies a difference in the  $g_{\text{eff}}^2 B_s$  product. We have taken, consistent with previous superconducting quantum interference device (SQUID) measurement, our  $\text{Ni}_{81}\text{Fe}_{19}$  films to have  $B_s=1.1$  T, fixing  $g_{\text{eff}}$  for the film at 2.03. The  $g_{\text{eff}}$  parameter has been fixed in the remainder of the fits. The assumption that most of the variation in the  $g^2 M_s$  product is contained in  $B_s$  is justifiable as  $g_{\text{eff}}$  values have been found to vary between 2.09 (Fe) and 2.2 (Ni), or a maximum of 5% in pure elements, whereas  $B_s$  values were found to vary by up to  $-20\%$  for 4% Gd addition in previous work.<sup>12</sup> In the present case, we find up to a 20% reduction in  $B_s$  for the largest Tb dose of  $1 \times 10^{15}/\text{cm}^2$ . Values of  $H_k$  did not change appreciably within experimental error. These values are summarized in Table I.

TABLE I. Calculated values of  $H_k$ ,  $B_s$ ,  $\alpha$ , and  $\Delta H_0$ .

Implant	$H_k$ (Oe)	$B_s$ (T)	$\alpha$	$\Delta H_0$ (Oe)
Undoped Py	$2.3 \pm 6$	1.1	0.008	$3 \pm 2$
Tb $1 \times 10^{14}$	$-6.3 \pm 6$	$1.067 \pm 0.007$	0.012	$-2 \pm 2$
Tb $5 \times 10^{14}$	$-5.8 \pm 6$	$1.002 \pm 0.005$	0.018	$4 \pm 3$
Tb $1 \times 10^{15}$	$24.8 \pm 22$	$0.893 \pm 0.03$	0.04	$-14 \pm 6$
Gd $1 \times 10^{14}$	$-2.0 \pm 6$	$1.072 \pm 0.005$	0.008	$4 \pm 1$

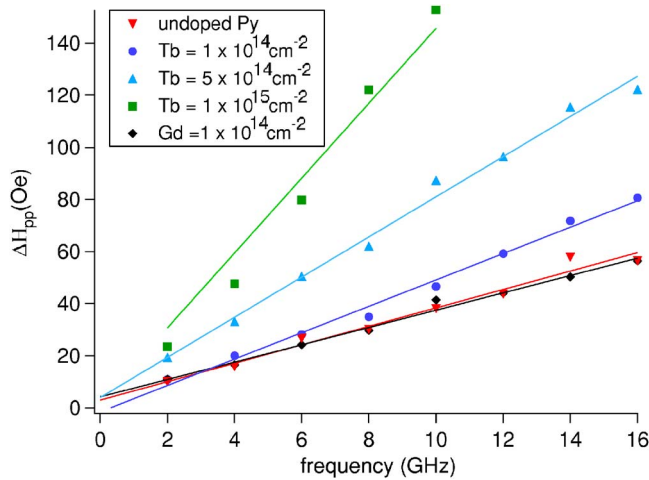


FIG. 3. (Color online) Extraction of homogeneous and inhomogeneous dampings for RE-implanted  $\text{Ni}_{81}\text{Fe}_{19}$ . Linear fits of  $\Delta H(\omega)$  are indicated, according to Eq. (2). Increases in  $\alpha$  from 0.008 to 0.04 are measured; no effect on inhomogeneous damping is observed.

Damping can be divided between homogeneous and inhomogeneous types. These types can be separated through variable-frequency FMR measurements of the field-swept linewidth  $\Delta H_{pp}$ , according to

$$\mu_0 \Delta H_{pp} = \frac{2}{\sqrt{3}} \frac{\alpha \omega}{\gamma} + \mu_0 \Delta H_0 \quad (2)$$

Homogeneous linewidth is proportional to frequency, described by the Landau-Lifshitz-Gilbert (LLG) parameter  $\alpha$  or rate  $G$ , equivalent for  $\alpha \ll 1$  to the LL rate  $\lambda$ . Inhomogeneous damping is constant with frequency, described by  $\Delta H_0$ , attributable in the coarsest sense to a locally varying anisotropy field for noninteracting regions.<sup>3</sup>

The variable-frequency FMR linewidths  $\Delta H_{pp}(\omega)$  for the implanted and control samples are shown in Fig. 3. Extracted values of  $\Delta H_0$  and  $\alpha$  are shown in Table I. There is a clear increase in slope with increasing Tb dose. Effects on the field offset are negligible within experimental error. The Gd dose has no measurable effect on damping, over the range studied.

## DISCUSSION

We find that the implanted Tb and Gd impurities retain their effective character on dynamics present in cosputtered alloys. The presence/absence of effects on damping for Tb/Gd dopants was attributed previously to the presence/absence of orbital moment on the RE site, Gd having a pure  $S$  state.<sup>1</sup>

The effectiveness of the dopants in enhancing damping,  $\Delta\alpha\%$ , corresponds reasonably with prior cosputtering experiments.<sup>12</sup> The nominal dosage of  $10^{15}$  ions/cm<sup>2</sup>, fully incorporated in the film, would correspond for  $\text{Ni}_{81}\text{Fe}_{19}$  (25 nm) to a dose of 0.5% Tb. In Ref. 12, we observed a  $\Delta\alpha\%$  of  $\sim 0.07$  for the series with best optimized magnetic

properties (low argon sputtering pressure). This would predict  $\alpha$  of 0.035 compared with the  $\alpha$  of 0.040 observed here.

The results provide further evidence that the effect of RE dopants is to contribute spin-lattice coupling, enhancing intrinsic (Gilbert type) damping. Separation of homogeneous and inhomogeneous contributions to linewidth had not been addressed in previous work, as pointed out in Ref. 3.

The ability to pattern precessional characteristics at sub-micron length scales, possible using focused ion beams or implantation through lithographic masks,<sup>13</sup> can enable magnetic nanostructures with high-speed phenomena. Spin-wave analogies of a photonic crystal (magnonic crystal) may be realizable through a periodic array of high- $\alpha$  regions. If the  $g_{\text{eff}}$  parameter can be manipulated locally, as has been indicated in studies on Eu dopants,<sup>1</sup> spin-wave refraction/lensing would be a possibility. For more immediate applications, it would be possible in a patterned [magnetoresistive random access memory (MRAM)] element to place high  $\alpha$  regions on edges, away from the center of an element, perhaps enabling more rapid full switching with a reduced impact on thermal noise, for which low  $\alpha$  is beneficial.<sup>14</sup>

## CONCLUSION

Rare-earth dopants Tb and Gd have been introduced into  $\text{Ni}_{81}\text{Fe}_{19}$  using ion implantation. Similar effects on precessional dynamics (damping  $\alpha$ ) have been observed as in samples created by cosputtering; these effects are demonstrated to be intrinsic properties of the dopants. The technique provides an additional degree of control over dynamics, enabling spatial manipulation of precession.

## ACKNOWLEDGMENTS

This work was partially supported by the ARO (ARO-43986-MS-YIP) and the NSF (NSF-DMR-02-39724). This work has used the shared experimental facilities that are supported primarily by the MRSEC program of the NSF under DMR-9809687.

- <sup>1</sup>S. Reidy, L. Cheng, and W. Bailey, *Appl. Phys. Lett.* **82**, 1254 (2003).
- <sup>2</sup>Y. Guan, Z. Dios, D. Arena, L. Cheng, and W. Bailey, *J. Appl. Phys.* **97**, 10A719 (2005).
- <sup>3</sup>B. Heinrich, *Ultrathin Magnetic Structures: Fundamentals of Nanomagnetism* (Springer, Berlin, 2005), Vol. III, Chap. 5, pp. 143–210.
- <sup>4</sup>J. Melngailis, *J. Vac. Sci. Technol. B* **5**, 469 (1987).
- <sup>5</sup>D. McGrouther and J. N. Chapman, *Appl. Phys. Lett.* **87**, 022507 (2005).
- <sup>6</sup>D. Ozkaya, R. M. Langford, W. L. Chan, and A. K. Petford-Long, *J. Appl. Phys.* **91**, 9937 (2002).
- <sup>7</sup>J. Katine, M. Ho, Y. S. Ju, and C. Rettner, *Appl. Phys. Lett.* **83**, 401 (2003).
- <sup>8</sup>J. Juraszek *et al.*, *J. Appl. Phys.* **91**, 6896 (2002).
- <sup>9</sup>J. McCord, T. Gemming, L. Schultz, J. Fassbender, M. Liedke, M. Frommberger, and E. Quandt, *Appl. Phys. Lett.* **86**, 162502 (2005).
- <sup>10</sup>A. Kos, T. Silva, and P. Kabos, *Rev. Sci. Instrum.* **73**, 3563 (2002).
- <sup>11</sup>J. Ziegler, SRIM, <http://www.srim.org>
- <sup>12</sup>W. Bailey, P. Kabos, F. Mancoff, and S. Russek, *IEEE Trans. Magn.* **37**, 1749 (2001).
- <sup>13</sup>M. Kuhn, B. Schey, R. Klarmann, W. Biegel, B. Stritzker, J. Eisenmenger, and P. Leiderer, *Physica C* **294**, 1 (1998).
- <sup>14</sup>N. Smith and P. Arnett, *Appl. Phys. Lett.* **78**, 1448 (2001).